

NONCOLLINEAR PHASE MATCHED FOUR PHOTON FREQUENCY MIXING IN WATER

A. PENZKOFER, J. KRAUS and J. SPERKA

*Naturwissenschaftliche Fakultät II - Physik, Universität Regensburg,
8400 Regensburg, Fed. Rep. Germany*

Received 29 January 1981

An intense ultraviolet picosecond light pulse at $\omega_S = 2\gamma_P - \omega_L$ is generated in water by noncollinear phase matched nonresonant four photon frequency mixing of two input picosecond light pulses at frequencies $\tilde{\nu}_P = 18\,960\text{ cm}^{-1}$ and $\tilde{\nu}_L = 9480\text{ cm}^{-1}$. An energy conversion of up to $W_S/W_L = 0.07$ was achieved. The nonlinear susceptibility components were determined to be $\chi_{yyyy}^{(3)}(-\omega_S; \omega_P, \omega_P, -\omega_L) = 7.5 \times 10^{-34}\text{ Cm/V}^3$ and $\chi_{yxyx}^{(3)}(-\omega_S; \omega_P, \omega_P, -\omega_L) = 2.4 \times 10^{-34}\text{ Cm/V}^3$.

1. Introduction

Four photon interactions are caused by the third order nonlinear polarization $\chi^{(3)}EEE$ which is the lowest order nonlinear polarization term in isotropic media [1–3]. Four photon frequency mixing processes may be resonantly enhanced when single frequencies, sum frequencies, or difference frequencies approach a transition frequency from initial state to an excited state [4,5]. The frequency mixing depends strongly on the phase mismatch between the involved waves [1–5] and optimum conversion efficiency is obtained for perfect phase matching.

In this letter nonresonant, noncollinear phase matched four photon frequency mixing [6,7] of picosecond light pulses in water is studied. A high conversion efficiency is obtained. The nonlinear susceptibility components are determined.

2. Theory

Input pulses of frequencies ω_P and ω_L generate light at $\omega_S = 2\omega_P - \omega_L$. The wave vector geometry is seen in fig. 1. The phase mismatch is defined as $\Delta k = k_S + k_L - 2k_P$. The electric field E_L is directed parallel to the y -axis while the electric field E_P is either parallel to the x -axis or to the y -axis.

The noncollinear frequency mixing is described by

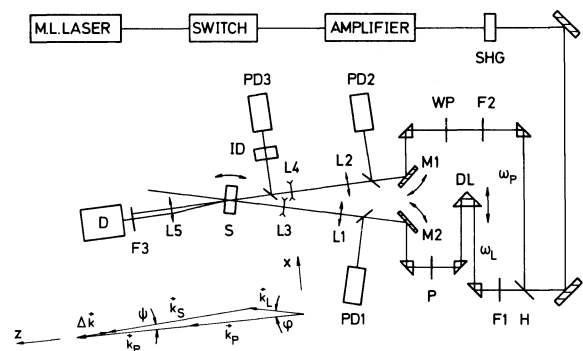


Fig. 1. Experimental setup. SHG, KDP crystal for second harmonic generation; H, harmonic beam splitter; F1–F3, filters; WP, $\lambda/2$ waveplate; DL, optical delay line; P, polarizer; M1, M2, plane mirrors; PD1–PD3, vacuum photocells, L1, L2 convex cylindrical lenses ($f = 30\text{ cm}$); L3, L4 concave cylindrical lenses ($f = -10\text{ cm}$). Composite focal lengths are $f(L1-L3) = 35\text{ cm}$ and $f(L2-L4) = 60\text{ cm}$. ID, two photon absorber CH_2I_2 (1 cm) for intensity detection; S, water sample; L5 collimating lens ($f = 10\text{ cm}$); D, optical multi-channel analyser or photodetector.

the wave equation [5]

$$\begin{aligned} \nabla^2 E - \frac{n^2}{c^2} \frac{\partial^2 E}{\partial t^2} - \frac{\partial n}{\partial t} \frac{\partial E}{\partial t} \\ = \mu_0 \left[\frac{\partial^2 P_{NL}}{\partial t^2} - \frac{c^2}{n^2} \nabla(\nabla \cdot P_{NL}) \right], \end{aligned} \quad (1)$$

n is the refractive index and α is the absorption coefficient. Eq. (1) is solved with the ansatz

$$A = \frac{1}{2} \sum_{\gamma=P,L,S} A_{\gamma} \exp[i(k_{\gamma}r - \omega_{\gamma}t)] + \text{c.c.}, \quad (2)$$

where A stands for E and P_{NL} . Using the slowly varying envelope approximation and the substitutions $z' = z, y' = y - (k_{\gamma y}/k_{\gamma z})z, x' = x - (k_{\gamma x}/k_{\gamma z})z, t' = t - (\omega_{\gamma}n_{g\gamma}/k_{\gamma z}c^2)z$ one obtains

$$\begin{aligned} \frac{\partial}{\partial z'} E_{\gamma} + \frac{n_{g\gamma}\alpha_{\gamma}\omega_{\gamma}}{2k_{\gamma z}c} E_{\gamma} \\ = \frac{i}{2k_{\gamma z}} \mu_0 \left[\omega_{\gamma}^2 P_{\text{NL},\gamma} - \frac{c^2}{n_{\gamma}^2} \mathbf{k}_{\gamma}(\mathbf{k}_{\gamma} \cdot P_{\text{NL},\gamma}) \right], \quad (3) \end{aligned}$$

$n_{g\gamma} = n_v/[1 + (\lambda_{\gamma}/n_{\gamma})\partial n_{\gamma}/\partial \lambda_{\gamma}]$ is the group refractive index at frequency ω_{γ} . Depletion of the input pulses is neglected in the mixing process and eq. (3) is only solved for E_S .

The nonlinear polarization is approximated by the lowest order nonlinear term of isotropic media $P_{\text{NL}} = \chi^{(3)}:EEE$. The symmetry properties of $\chi^{(3)}$ [2,5] together with the polarization of the input laser pulses ($E_L \parallel y$ -axis, $E_P \parallel y$ or x -axis) lead to

$$\begin{aligned} P_{\text{NL},S,y} = \frac{3}{4} \chi_{yyyy}^{(3)}(-\omega_S; \omega_P, \omega_P, -\omega_L) \\ \times E_P^2 E_L^* \exp(-i\Delta k r) \end{aligned} \quad (4)$$

and

$$P_{\text{NL},S,x} = P_{\text{NL},S,z} = 0$$

($j = x$ for $E_P \parallel x, j = y$ for $E_P \parallel y, \mathbf{k}_S \perp P_{\text{NL},S}$).

Integration of eq. (3) with the initial condition

$$E_S(z=0) = 0 \text{ gives}$$

$$\begin{aligned} E_S(x', y', t', l) \\ = i \frac{3\mu_0\omega_S c}{8n_S \cos(\psi)} \chi_{yyyy}^{(3)} \exp(-i\Delta k_x x') \\ \times \int_0^l E_P^2(x', y', t', z) E_L^*(x', y', t', z) \\ \times \exp\left\{-i[\Delta k_z - \Delta k_x \tan(\psi)]z - \frac{n_{gS}\alpha_S(l-z)}{2n_S \cos(\psi)}\right\} dz, \end{aligned} \quad (5)$$

where $k_{Sz} = n_S\omega_S \cos(\psi)/c$ and $x = x' - \tan(\psi)z$ are used ($E_{Sy} = E_S, E_{Sx} = E_{Sz} = 0$). The phase mismatch is $\Delta k_x = k_L \sin(\varphi) - k_S \sin(\psi)$ and $\Delta k_z = k_L \cos(\varphi) + k_S \cos(\psi) - 2k_P$. The pump pulse amplitudes are

$$\begin{aligned} E_P(x, y, z, t) = E_{0P} \exp\left\{-\frac{1}{2}[x^2/x_P^2 + y^2/y_P^2 \right. \\ \left. + (t - n_{gP}z/c)^2/t_P^2 + \alpha_P z]\right\}, \end{aligned} \quad (6)$$

and

$$\begin{aligned} E_L(x, y, z, t) \\ = E_{0L} \exp\left(-\frac{1}{2}\{[x \cos(\varphi) - (z - l/2) \sin(\varphi)]^2/x_L^2 \right. \\ \left. + y^2/y_L^2 + [t - t_D - n_{gL}(x \sin(\varphi) + z \cos(\varphi))/c]^2/t_L^2 \right. \\ \left. + \alpha_L [x \sin(\varphi) + z \cos(\varphi)]\right\}. \end{aligned} \quad (7)$$

In eq. (7) a coordinate transformation of E_L to the x, y, z -frame of E_P is performed. The pump beams cross in the center of the cell due to term $(l/2) \sin(\varphi)$ in eq. (7). t_D represents the temporal separation of the input pulses.

The intensity of the generated light signal is obtained from eq. (5) by averaging E_S over fast changes in the x' direction [15] and by forming the absolute square $I_S = n_S c \epsilon_0 |E_S|^2/2$. The generated signal energy is calculated by integration over space and time

$$W_S = \int_{-\infty}^{\infty} \int_{-\infty}^{\infty} \int_{-\infty}^{\infty} I_S dx' dy' dt'$$

and finally, the energy conversion $\eta = W_S/W_L$ is defined as the ratio of generated energy at ω_S to input energy at ω_L . The experimental parameters involved in the calculations are summarized in table 1.

3. Experiments

The experimental setup is depicted in fig. 1. A mode locked Nd-phosphate glass laser is used [8]. Single light pulses are selected with an electrooptical switch and increased in energy with an amplifier. The pulses have a duration of $\Delta t_L \approx 6$ ps (FWHM) and a spectral width of $\Delta \tilde{\nu}_L \approx 10 \text{ cm}^{-1}$ (FWHM). The second harmonic is generated in a KDP crystal (length 1 cm). The fundamental laser pulse ($\tilde{\nu}_L = 9480 \text{ cm}^{-1}$) and the second harmonic ($\tilde{\nu}_P = 18960 \text{ cm}^{-1}$) act as

Table 1
Laser and material parameters

Frequencies		
$\tilde{\nu}_L = 9\,430\text{ cm}^{-1}$;	$\tilde{\nu}_P = 18\,960\text{ cm}^{-1}$;	$\tilde{\nu}_S = 28\,440\text{ cm}^{-1}$
Pulse durations		
$t_L = \Delta t_L / (2\sqrt{\ln(2)}) = 3.6\text{ ps}$; $t_P = 3\text{ ps}$		
Beam cross-sections		
$x_L = \Delta x_L / (2\sqrt{\ln(2)}) = 4.2\text{ mm}$;	$x_P = 2.85\text{ mm}$	
$y_L = 0.065\text{ mm}$;	$y_P = 0.071\text{ mm}$	
Beam divergence		
outside cell		
$2\theta'_L = 4 \times 10^{-4}$	$2\theta'_P = 2 \times 10^{-4}$	$2\theta'_{S,xz} = 4.4 \times 10^{-4}$
inside cell ($2\theta = 2\theta' \cos(\varphi'_{\text{opt}}) / [n \cos(\varphi_{\text{opt}})]$)		
$2\theta_L = 3 \times 10^{-4}$	$2\theta_P = 1.6 \times 10^{-4}$	$2\theta_{S,xz} = 3.3 \times 10^{-4}$
Refractive indices at 25°C [10]		
$n_L = 1.3247$	$n_P = 1.33468$	$n_S = 1.34815$
$n_{gL} = 1.33518$	$n_{gP} = 1.35783$	$n_{gS} = 1.39823$
Absorption coefficients [11]		
$\alpha_L = 0.133\text{ cm}^{-1}$	$\alpha_P = 3.2 \times 10^{-4}\text{ cm}^{-1}$	$\alpha_S = 2.3 \times 10^{-3}\text{ cm}^{-1}$

input pulses in the frequency mixing process.

The picosecond pulses at frequencies ω_P and ω_L are separated with a harmonic beam splitter H. The optical delay line DL adjusts the pulses for temporal overlap in the sample. The angle φ' between the input beams (outside sample) is changed by translation and rotation of the mirrors M1 and M2. The composite cylindrical lenses L1, L3 and L2, L4 form line focuses in the sample S. The beam extension in x -direction assures spatial overlap of the waves over a long distance (ca. 3 cm). Fine tuning of the angle φ (inside cell) is achieved by twisting the sample. The change of refraction angle between input beams is approximately 0.01° for cell rotation of 1° .

The peak intensity of the input pulses at frequency ω_P is monitored by two-photon transmission measurements through methyl iodide ID with photo-cells PD2 and PD3 [9]. The pulse energy at frequency ω_L is measured with the calibrated photodetector PD1. The generated light at frequency $\tilde{\nu}_S = 28\,440\text{ cm}^{-1}$ is detected either with an optical multichannel analyser (energy and space resolution) or with a calibrated photodetector.

A $\lambda/2$ wave plate WP is used to orient E_P parallel to E_L (coupling constant $\chi_{yyyy}^{(3)}$). Without the waveplate,

E_P is directed in the x -direction (coupling constant $\chi_{yyxy}^{(3)}$). Polarizer P establishes perfect polarization of E_L in y -direction.

4. Results

The angular dependence of the energy conversion $\eta = X_S W_L$ is depicted in fig. 2. The dashed curve $\eta(\varphi)/\eta(\varphi_{\text{opt}})$ is calculated with the aid of eq. (5). The solid curve is obtained by convolution of the dashed curve with the angular intensity distribution of the input lasers. The optimum energy conversion is reduced by the divergence of the input beams by a factor of 0.65. The experimental points (\circ) are adjusted to the calculated curves at the theoretical phase matching angle $\varphi_{\text{opt}} = \arccos\{[(2k_P)^2 + k_L^2 - k_S^2] / (4k_P k_L)\} = 10.685^\circ$ ($\Delta k = 0$). Experimentally, an angle of $\varphi_{\text{opt}} = 10.63^\circ \pm 0.08^\circ$ ($\varphi'_{\text{opt}} = 14.15^\circ \pm 0.1^\circ$ outside water) was found. The angular spread of the phase matching angle is $\Delta\varphi_{\text{opt}} = 0.024^\circ = 4.2 \times 10^{-4}$ rad (FWHM).

The angle ψ between k_P and k_S is given by the wave-vector triangle included in fig. 1. (Deviation from a triangular geometry increases $|\Delta k|$). One finds $\psi = \arccos$

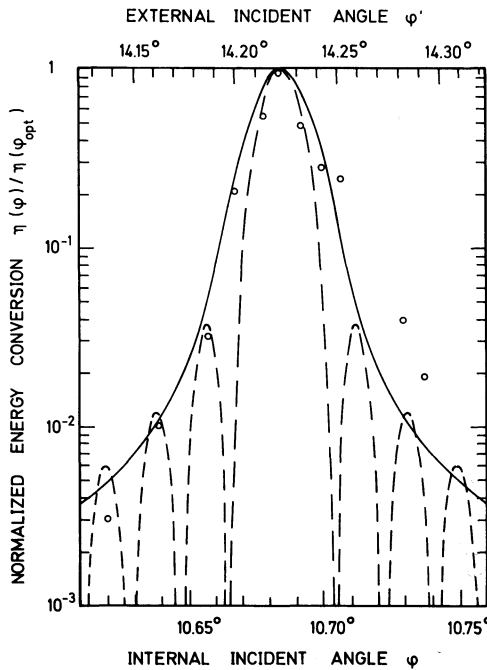


Fig. 2. Angular dependence of energy conversion. Dashed curve, calculated with aid of eq. (5). Solid curve, convolution of dashed curve with angular intensity distribution of input pulses (see table 1). The data points are adjusted to position of peak conversion. External incident angle ϕ' is calculated for cell orientation normal to bisector of input beams ($\phi = \arcsin [(1/n_L) \sin(\phi'/2)] + \arcsin [(1/n_P) \sin(\phi'/2)]$).

$\sin \{k_L \sin(\phi) / [k_L^2 + (2k_P)^2 - 4k_P k_L \cos(\phi)]^{1/2}\}$. For perfect phase matching the angle of emission is $\psi_{opt} = \arcsin [k_L \sin(\phi) / k_S] = 3.48^\circ$ ($\psi'_{opt} \approx 4.85^\circ$ outside sample).

The divergence of the generated light in the xz -plane was measured with an optical multichannel analyser positioned in the focal plane of lens L5 (see fig. 1). A divergence $2\theta'_{S,xz} = 4.4 \times 10^{-4}$ rad was found.

At large phase mismatch angles $|\phi - \phi_{opt}| > 0.5^\circ$ light of frequency ω_S is observed at three emission angles. The strongest beam is radiated in the above described direction. The two other beams are due to phase matched interaction of one input pulse with stray light of the other input pulse [12].

The dependence of the energy conversion on the input peak intensity I_{OP} is shown in fig. 3 for various sample lengths. The calculated curves and measured data points are presented for perfect phase matching.

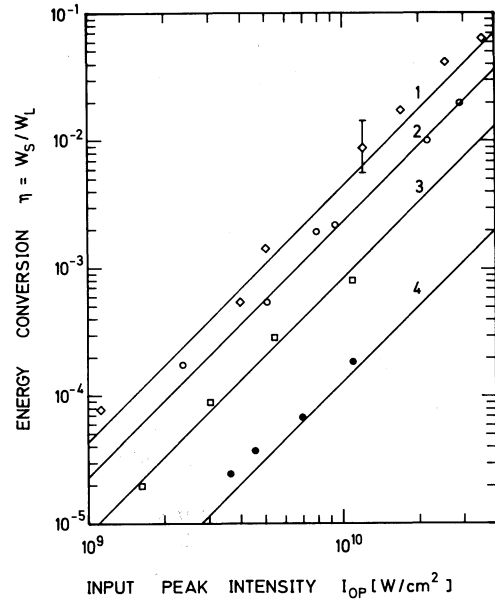


Fig. 3. Energy conversion versus input peak intensity I_{OP} for various sample lengths at perfect noncollinear phase-matching. $E_P \parallel E_L \parallel y$ -axis. Sample lengths $l = 2$ cm (1, \diamond), $l = 1$ cm (2, \circ), $l = 0.5$ cm (3, \square) and $l = 0.2$ cm (4, \bullet). Curves are calculated for $\chi_{yyyy}^{(3)} = 7.5 \times 10^{-34}$ Cm/V³.

At a fixed cell length the energy conversion increases quadratically with I_{OP} . At $I_{OP} = 4 \times 10^{10}$ W/cm² an energy conversion of $\eta \approx 0.07$ was obtained in a water cell of 2 cm length ($I_{OL} \approx 5 \times 10^8$ W/cm²). For $I_{OP} > 2 \times 10^{10}$ W/cm² the four photon interaction is more complex than described by eq. (5): i) The frequency mixing process $2\omega_P - \omega_L \rightarrow \omega_S$ changes over to the parametric interaction process $\omega_P + \omega_P \rightarrow \omega_L + \omega_S$ where light at frequencies ω_L and ω_S is amplified (complete equation system 3 should be solved) [13,14]. ii) When $I_{OL} \geq I_{OP}$ depletion of the pump pulse at ω_P has to be taken into account. At $I_{OP} = 3 \times 10^{10}$ W/cm² the energy conversion reduced from $\eta = 0.05$ for $I_{OL} \approx 5 \times 10^8$ W/cm² to 0.035 for $I_{OL} \approx 3 \times 10^{10}$ W/cm². For $I_{OL} > 5 \times 10^{10}$ W/cm² light at frequency ω_L is reduced by generation of broad band picosecond light continua due to parametric four photon interaction [13,16].

At a fixed input intensity I_{OP} the energy conversion increases quadratically with sample length up to a length of 1 cm. For longer cells the conversion levels down since the spatial overlap of the noncollinear input beams is limited to about 3 cm. For cell lengths

longer than 3 cm and optimum overlap in the center of the cell the conversion η reduces gradually since the input pulse at ω_L is slightly absorbed in water.

The duration of the generated light at ω_S is determined by the temporal overlap of the input pulses. Calculations of $I_S(t)$ indicate a pulse duration of $\Delta t_S \approx 3.5$ ps (FWHM).

The spectral width of the generated light was measured with a 0.6 m spectrograph and an optical multi-channel analyser. A spectral width of $\Delta \tilde{\nu}_S \approx 10$ cm⁻¹ was found.

The polarization of the output light at ω_S was analyzed with a polarizer behind the sample. In case of $E_P \parallel E_L \parallel y$ a depolarization ratio of $E_{S,x}^2/E_{S,y}^2 \leq 0.075$ was measured (coupling constant $\chi_{yyyy}^{(3)}$). For $E_P \parallel x$ and $E_L \parallel y$ the depolarization was $E_{S,x}^2/E_{S,y}^2 \leq 0.12$ (coupling constant $\chi_{yxxxy}^{(3)}$). Theory predicts $E_{S,x}^2/E_{S,y}^2 = 0$ ($E_S \parallel y$) in both cases (see eq. (4)).

The quantitative analysis of the frequency mixing process allows the determination of the nonlinear susceptibility tensor $\chi^{(3)}$. In isotropic media the $\chi^{(3)}$ -tensor has three independent components $\chi_{yyyy}^{(3)}$, $\chi_{yxxxy}^{(3)}$ and $\chi_{xyxyx}^{(3)}$ [2,5]. In our case two frequencies are equal and only two components are independent [$\chi_{xyxyx}^{(3)} = \chi_{yxyxx}^{(3)} = (\chi_{yyyy}^{(3)} - \chi_{yxxxy}^{(3)})/2$]. The two components $\chi_{yyyy}^{(3)}$ and $\chi_{yxxxy}^{(3)}$ are determined by comparing the measured energy conversion with calculation. We found $|\chi_{yyyy}^{(3)}(-\omega_S; \omega_P, \omega_P, -\omega_L)| = (7.5 \pm 2) \times 10^{-34}$ Cm/V³ = $(6 \pm 1.5) \times 10^{-15}$ esu ($E_P \parallel E_L \parallel y$) and $|\chi_{yxxxy}^{(3)}(-\omega_S; \omega_P, \omega_P, -\omega_L)| = (2.4 \pm 0.6) \times 10^{-34}$ Cm/V³ = $(1.9 \pm 0.5) \times 10^{-15}$ esu ($E_P \parallel x$, $E_L \parallel y$). The obtained $\chi^{(3)}$ -values are in satisfactory agreement with previously reported nonresonant susceptibility values of water at different frequencies [17-19].

Acknowledgement

The authors are indebted to Dr. J. Wiedmann for

initial measurements and to Prof. M. Maier for helpful discussions. They are grateful to the Deutsche Forschungsgemeinschaft for financial support.

References

- [1] J.A. Armstrong, N. Bloembergen, J. Ducuing and P.S. Pershan, *Phys. Rev.* 127 (1962) 1918.
- [2] P.N. Butcher, *Nonlinear optical phenomena* (Ohio State University, Ohio, 1965).
- [3] N. Bloembergen, *Nonlinear optics* (Benjamin, New York, 1965).
- [4] R.W. Terhune and P.D. Maker, *Lasers*, Vol. 2, Ch. 4, ed. A.K. Levine (Marcel Dekker, New York, 1968).
- [5] C. Flytzanis, *Quantum electronics*, Vol. 1, Ch. 2, eds. H. Rabin and C.L. Tang (Academic Press, New York, 1975).
- [6] D.H. Auston, *Appl. Phys. Letters* 18 (1971) 250.
- [7] D.H. Auston, *Optics Comm.* 3 (1971) 272.
- [8] A. Laubereau and W. Kaiser, *Opto-Electronics* 6 (1974) 1.
- [9] A. Penzkofer and W. Falkenstein, *Optics Comm.* 17 (1976) 1.
- [10] A.M. Hellwege, *Landolt-Börnstein*, 6th Edition, Vol. 2, Part 8, eds. K.H. Hellwege and A.M. Hellwege (Springer-Verlag, Berlin, 1962).
- [11] G.M. Hale and M.R. Querry, *Appl. Optics* 12 (1973) 555.
- [12] J.A. Giordmaine, *Phys. Rev. Letters* 8 (1962) 19.
- [13] A. Penzkofer and W. Kaiser, *Opt. Quant. Electron* 9 (1977) 315.
- [14] A. Penzkofer, A. Laubereau and W. Kaiser, *Prog. Quant. Electr.* 6 (1979) 55.
- [15] G.D. Boyd, A. Ashkin, J.M. Dziedzic and D.A. Kleinman, *Phys. Rev.* 137 (1965) A1305.
- [16] A. Penzkofer, A. Seilmeier and W. Kaiser, *Optics Comm.* 14 (1975) 363.
- [17] P.D. Maker and R.W. Terhune, *Phys. Rev.* 137 (1965) 801.
- [18] D.L. Weinberg, *Appl. Phys. Letters* 14 (1969) 32.
- [19] M. Becker, R. Fischer, J. Frahm, R. Güther and H. Stuedel, *Opt. Quant. Electron* 6 (1976) 279.